Since January 2020 Elsevier has created a COVID-19 resource centre with free information in English and Mandarin on the novel coronavirus COVID-19. The COVID-19 resource centre is hosted on Elsevier Connect, the company's public news and information website.

Analytical Biochemistry 657 (2022) 114898

Contents lists available at ScienceDirect

Analytical Biochemistry

journal homepage: www.elsevier.com/locate/yabio

Discriminative electrochemical biosensing of wildtype and omicron variant of SARS-CoV-2 nucleocapsid protein with single platform

Lokman Liv *, Aysu Baş

Electrochemistry Laboratory, Chemistry Group, The Scientific and Technological Research Council of Turkey, National Metrology Institute, (TUBITAK UME), 41470, Gebze, Kocaeli, Turkey

ARTICLE INFO

Keywords:
COVID-19
SARS-CoV-2
Omicron variant
Nucleocapsid antigen protein
Electrochemical biosensing platforms
Voltammetry

ABSTRACT

Electrochemical biosensors for determining wildtype and omicron variant of the severe acute respiratory syndrome-coronavirus-2 (SARS-CoV-2) nucleocapsid antigen in nasopharyngeal swab samples were produced by using functionalised graphene oxide and the wildtype and omicron types of SARS-CoV-2 nucleocapsid antibody modified glassy carbon electrodes. The developed biosensors characterised by cyclic voltammetry, scanning electron microscopy, energy dispersive X-ray spectroscopy and X-ray photoelectron spectroscopy were able to detect 0.76 and 0.24 ag/mL of the wildtype and omicron SARS-CoV-2 nucleocapsid antigen protein in linear ranges varied from 1 ag/mL to 100 fg/mL and from 1 ag/mL to 10 fg/mL, respectively. The performance of both biosensors produced was compared in nasopharyngeal swab samples containing the wildtype and omicron variant of the SARS-CoV-2, and it was evaluated whether they could be used interchangeably.

1. Introduction

The unparagoned coronavirus disease 2019 (COVID-19) has heavily ruined public health systems and economies worldwide [1,2]. In addition to the large amounts of money spent by countries with the COVID-19 pandemic, global debt has also increased from $226 trillion in 2020 to $303 trillion in 2021. According to the IMF, this is the highest amount reached after the Second World War [3]. Apart from the fiscal issues, as of 1 June 2022, more than 527.6 million confirmed cases of COVID-19 and 6.29 million deaths have been tallied by the World Health Organization (WHO) [4].

SARS-CoV-2, a member of *betacoronavirus* genus, has a tendency to genetic evolution while adapting to new human hosts with the development of mutations in time, like other RNA viruses. This has led to the appearance of various variants that might have different features in comparison to their hereditary strains [5]. The WHO has classified the SARS-CoV-2 variants as alpha, beta, gamma, delta and omicron (variants of concern, VOCs) and has announced that delta and omicron variants are in circulation as of May 2022 [6]. The studies show that the omicron variant has a 13-fold increase in viral infection and this variant is 2.8 times more contagious than the delta variant [7]. It was determined that the efficacy of ChAdOx1 nCoV-19, BNT162b2 and mRNA-1273 vaccines against the omicron variant was lower than the delta variant at all post-vaccination intervals and in all primary and booster dose combinations investigated [8]. This situation also affected the diagnosis of the disease, and especially with the emergence of the omicron variant, the need to revise RT-PCR kits, rapid antigen test kits and biological materials sensitive to the omicron variant used in biosensors has arisen [9].

Diagnosis of COVID-19 is mostly based on real-time polymerase chain reaction (RT-PCR) distinguishing the genetic material of the virus in bodily fluids including saliva, oropharyngeal and nasopharyngeal swab samples. RT-PCR has advantages involving being sensitive and selective, whereas it entails a long assay time and an expensive instrument [10–12]. Other commonly used diagnostic methods include lateral flow immunoassay (LFIA) [13–15], serological tests such as enzyme-linked immunosorbent assay (ELISA) [16], and electrochemical biosensors [17–25]. LFIA– and ELISA–based methods have mentioned benefits such as cheap, rapid and easy-to-use, whilst LFIA–based methods have lower sensitivity and ELISA–based methods are not proper for early diagnosis since they detect antibodies against viral antigens [16,26]. By comparison, electrochemical methods have demonstrated many benefits involving ease of use, cost-effective and rapid analysis, high sensitivity and selectivity. Thus, electrochemical studies for the diagnosis of infectious diseases including COVID-19 are constantly increasing, the featured ones are compiled in Table S1 [17–25].

* Corresponding author.
E-mail address: lokman.liv@tubitak.gov.tr (L. Liv).

https://doi.org/10.1016/j.ab.2022.114898
Received 11 July 2022; Received in revised form 31 August 2022; Accepted 6 September 2022
Available online 11 September 2022

However, among these methods, the production of biosensors for the simultaneous detection of wildtype and omicron variant of the SARS-CoV-2 in real samples and whether these sensors can be used interchangeably have not been investigated up to now.

We here produced two biosensing platforms obtained by modifying the wildtype and the omicron nucleocapsid antibodies onto functionalised graphene oxide modified electrodes for determining the wildtype and the omicron variant of the less mutated SARS-CoV-2 nucleocapsid antigen proteins in nasopharyngeal swab samples. To the best of our knowledge, this is the first electrochemical comparative study to simultaneously detect nucleocapsid proteins of both the wildtype and the omicron variant of the SARS-CoV-2 in real samples.

2. Material and methods

2.1. Chemicals and equipment

The SARS-CoV-2 (2019-nCoV) nucleocapsid-his recombinant protein (wAG, >90% as determined by SDS-PAGE, Cat: 40588-V08B), SARS-CoV-2 B.1.1.529 (omicron) nucleocapsid protein (his tag) (oAG, >95% as determined by SDS-PAGE and SEC-HPLC, Cat: 40588-V07E34), SARS-CoV-2 nucleocapsid antibody (wAB, validated by WB and ELISA, Rabbit MAb Cat: 40143-R019), SARS-CoV-2 omicron nucleocapsid antibody (oAB, validated by WB, ELISA, IHC-P and ICC/IF, Rabbit MAb Cat: 40143-R001), influenza A H1N1 Hemagglutinin/H0A protein (A/Guangdong-Maonan/SWL1536/2019)/(A/Hawaii/70/2019) (his-tag) (>95% as determined by SDS-PAGE, Cat: 40717-V08H) and the Middle East respiratory syndrome-coronavirus (MERS-CoV) nucleocapsid protein (his-tag) (>90% as determined by SDS-PAGE, Cat: 40068-V08B) were purchased from Sino Biological, and the native extract of *Streptococcus pneumoniae* antigen (inactivated antigen from culture, NAT41604-100) was supplied from Native Antigen Company. Graphene oxide (GO, Powder, Sigma-Aldrich 796034), phosphate-buffered saline (PBS, tablet, Sigma-Aldrich, P4417, 0.01 M phosphate buffer, 0.0027 M potassium chloride and 0.137 M sodium chloride, pH 7.5, at 25 °C), N-Hydroxysuccinimide (NHS, 98%, Sigma-Aldrich 130672), N-(3-Dimethylaminopropyl)-N′-ethylcarbodiimide hydrochloride (EDC, ≥98, Sigma-Aldrich 03450) and bovine serum albumin (BSA, ≥98%, Sigma-Aldrich, 05470) were purchased from Sigma-Aldrich, USA. 0.01 M (pH 7.5) of PBS solution and Eppendorf protein LoBind tubes were used to prepare and store the antibody and antigen solutions, respectively. The other chemicals were dissolved in ultrapure water.

Thermo Scientific HiPPR Detergent Removal Spin Column Kit (Cat: 88305) was used to remove detergent from the nasopharyngeal swab samples.

Merck Millipore Milli-Q Integral 10 system was used to procure ultrapure water, ISOLAB 3 L ultrasonic bath was operated to clean the surface of glassy carbon electrode (GCE) and General Electric 250W infrared lamp (E27, 125 mm) were utilized to evaporate the ultrapure water and dry the graphene oxide suspension onto the GCE.

Voltammetric measurements were performed using Metrohm Autolab PGSTAT 128 N potentiostat/galvanostat with a three-electrode system consisting of working electrodes (the wildtype or the omicron nucleocapsid antibody and functionalised graphene oxide modified glassy carbon electrode, BASi MF-2012 GCE as a supporting surface), reference (Ag/AgCl/3 M NaCl, BASi MF-2052 RE-5B) and counter (platinum wire, BASi MW-1032, 7.5 cm) electrodes.

Biorad CFX Connect Real-Time PCR system was used to analyse the nasopharyngeal swab samples.

Hitachi Schottky SU5000 field emission-scanning electron microscope (FE-SEM), FEI Oxford Instruments Model 7260 energy dispersive X-ray spectroscopy (EDX) and Thermo Fisher K-Alpha X-ray photoelectron spectroscopy (XPS) were operated to characterise the biosensing platforms.

2.2. Preparation of the SARS-CoV-2 wildtype and omicron variant biosensing platforms

To prepare the wildtype SARS-CoV-2 nucleocapsid antibody (wAB) modified electrode, first the surface of GCE was orderly lustered with 0.5, 0.3 and 0.1 μm of diamond paste on the felt and washed with ultrapure water, subsequently ultrasonicated in a 1:1 ethanol–ultrapure water mixture taken turns with ultrapure water for 5 min each. Then, 3 μL of 2.5 mg/mL GO suspension was dropped onto the GCE surface, dried under an infrared lamp and allowed to cool for 15 min. Next, 6 μL of 100 mM EDC and 14 μL of 100 mM NHS were dropped onto the GO/GCE surface for 1.5 h to activate the electrode surface and to ease the wAB immobilisation for the further step (*a*GO/GCE). Finally, after incubating 10 μL of the 20 ppm wAB on the *a*GO/GCE surface for 30 min, the free sites were blocked with 10 μL of 2% BSA. The obtained platform was denoted as BSA/wAB/*a*GO/GCE (Fig. 1).

To prepare the omicron SARS-CoV-2 nucleocapsid antibody (oAB) modified electrode, the sequence of the biosensor preparation steps was the same, only the ratios of EDC and NHS were 16 μL and 4 μL, respectively, and the activation time is 30 min. Apart from that, oAB was used instead of wAB for antibody immobilisation. The obtained platform was denoted as BSA/oAB/*a*GO/GCE (Fig. 1).

The incubations were carried out at 21 ± 3 °C and the prepared platforms were stored in a cooler at 4 °C until further use. At the end of each of the sensor preparation steps, washing was made with the solution in which the modified material was prepared, and then the surface was dried with high purity argon gas.

2.3. Voltammetric measurements

The wildtype (wAG) or the omicron variant nucleocapsid antigen (oAG) was incubated on the related biosensing platform for 45 min before being measured. Square wave voltammetry (SWV) was applied in the potential range between −1 V and 1 V with 5 mV of step amplitude, 10 Hz of frequency and 25 mV of pulse amplitude. Cyclic voltammetry (CV) was performed in the same potential range with 3 mV of step amplitude and an appropriate scan rate. All electrochemical measurements were recorded in a supporting electrolyte solution containing 0.01 M (pH 7.5) of PBS degassed with argon for 5 min before the measurement. The anodic peaks of the produced platforms increased at approximately −60 mV in proportion to wAG and oAG, which were used for determining wAG and oAG.

2.4. Clinical analyses

Nasopharyngeal swab samples (30 negative and 30 positive samples for wAG detection, 25 negative and 25 positive samples for oAG detection) collected in the first quarters of 2020 and 2022 and confirmed by RT-PCR were used for determining wAG and oAG, respectively. The selection of these samples was carried out randomly from approximately 300 nasopharyngeal swab samples for each variant and each positive and negative samples using the TRaNS (Stratified Random Sample Selection) software. Ethical approvals for wAG and oAG studies were obtained from Acibadem University Ethical Committee with IDs of ATADEK 2020–14/2 and ATADEK 2021–24/34, also respectively.

2.5. Sample preparation for voltammetric analyses

First, nasopharyngeal swab samples in detergent solution marked positive or negative and confirmed by RT-PCR were cleaned of detergent in order to reveal the nucleocapsid proteins. For this purpose, 200 μL of detergent removal resin was added into spin columns with stoppers. Next, the stoppers were removed and spin columns were placed in Eppendorf tubes, centrifuged at 2000 rpm for 1 min at room temperature, and the liquid collected in Eppendorf tubes was discarded. After 200 μL of 0.01 M (pH 7.5) PBS solution was added into the spin columns,

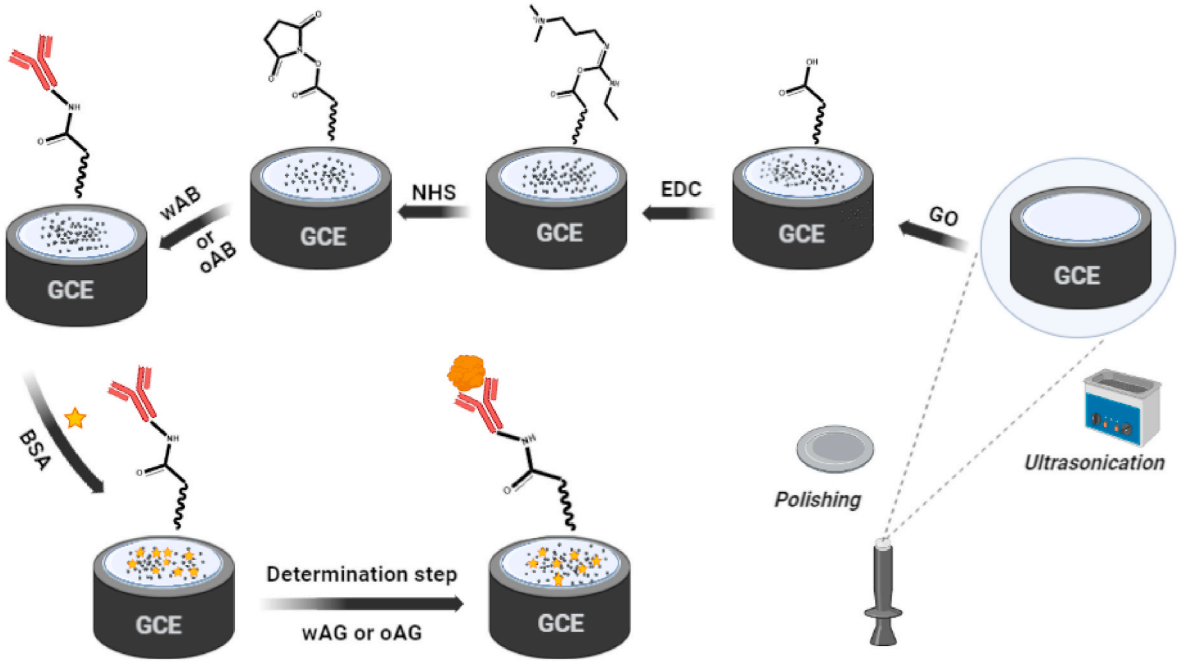

Fig. 1. Schematic presentation of the procedures for preparing wildtype and omicron variant biosensing platforms.

the resin was washed by centrifuging at 2000 rpm for 1 min. This process was repeated 3 times and the liquid collected in Eppendorf tubes was discarded each time. Then, the resin-cleaned spin columns were placed inside the clean Eppendorf tubes with stoppers. Nasopharyngeal swab samples with a volume of 100 μL were added onto the resin, pipetted 3 times and incubated for 10 min at room temperature. At the end of the incubation, the stoppers were opened and the samples were centrifuged at 2000 rpm for 1 min. After centrifugation, the supernatants of nasopharyngeal swab samples without detergent were transferred to +4 °C. Those RT-PCR confirmed samples were incubated on the biosensor surfaces with a volume of 5 μL and used for the determination of wAG and oAG and hence for the diagnosis of COVID-19. The whole sample preparation and measurement procedure is summarized in Fig. 2.

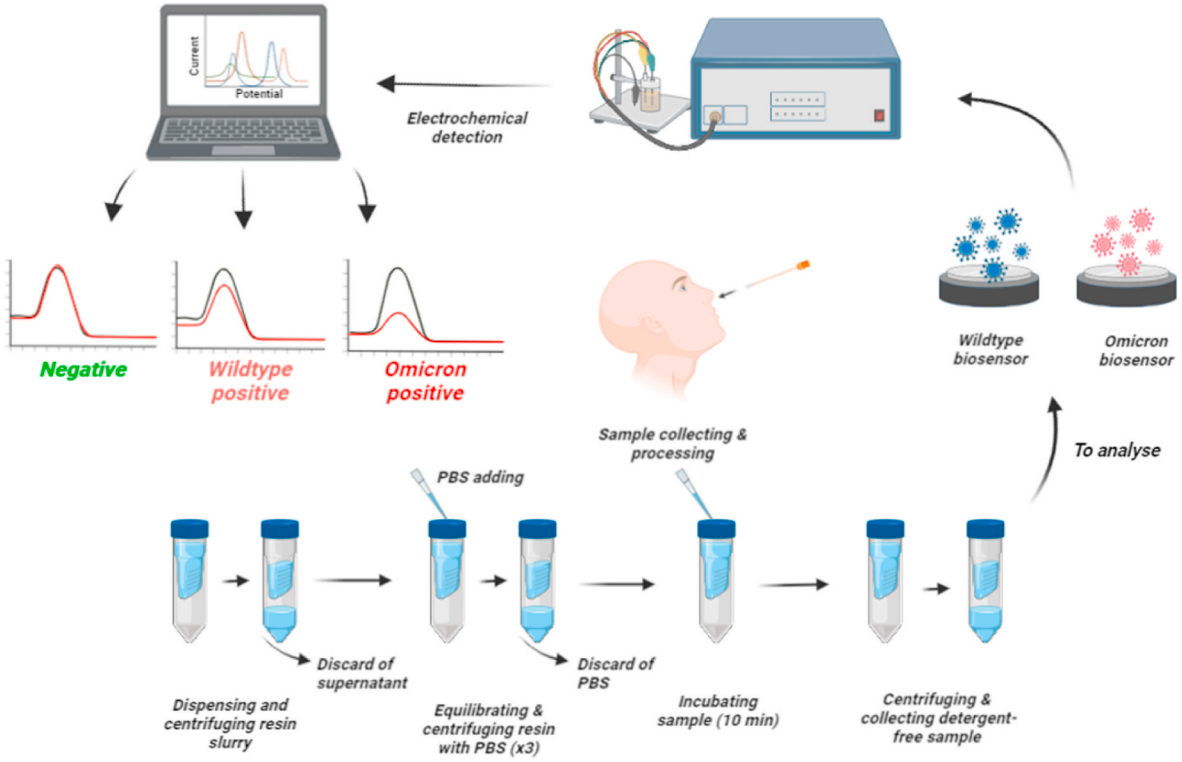

Fig. 2. Schematic presentation of the sample preparation and measurement procedure.

3. Results and discussion

3.1. Surface characterisation of the produced platforms

Surfaces of the produced biosensors were characterised by CV, FE-SEM, EDX and XPS to identify each modification of the BSA/wAB/*a*GO/GCE and BSA/oAB/*a*GO/GCE. Cyclic voltammograms of the GCE, GO/GCE, *a*GO/GCE, wAB/*a*GO/GCE, oAB/*a*GO/GCE, BSA/wAB/*a*GO/GCE and BSA/oAB/*a*GO/GCE in the presence of 1 mM of $K_3[Fe(CN)_6]$, 1 mM of $K_4[Fe(CN)_6]$ and 0.1 M of KCl as shown in Fig. 3.

The peak heights of the redox couple remarkably increased owing to the enhancing surface area and hence the electron transfer rate after the GO modification onto the GCE surface (Fig. 3A–a and b, 3B-a and b). After activation of GO with EDC and NHS, since unpaired electrons found in the carbonyl of NHS faced the outside of the electrode, the peak intensities decreased due to the repulsion forces between the carbonyl groups and the redox couple as appear in Fig. 3A–c and 3B-c. With wAB and BSA modified on the *a*GO/GCE, it was observed that the peak heights first increased and then decreased (Fig. 3A–d and e). The former is based on the electrostatic attraction between the amino groups in the wAB and the negatively charged redox couple, whereas the latter arises from the high concentration of BSA and due to the fact that a physical barrier is encountered for the redox couple to reach the electrode surface. These findings are in full agreement with the results of our previous study [18]. Unlike this study, the peak intensities decreased when oAB was modified on the *a*GO/GCE surface (Fig. 3B–d). This is due to the fact that wAB, the ancestor of oAB, has undergone numerous phosphorylation and therefore, there have been changes in its conformation and possibly occurred negative charges on its surface [27]. The repulsion forces between these negative charges and the redox couple or steric hindrance due to the oAB structure caused a decrease in the peak heights. The peak heights continued to lessen with the BSA immobilisation similar to the BSA/wAB/*a*GO/GCE (Fig. 3B–e).

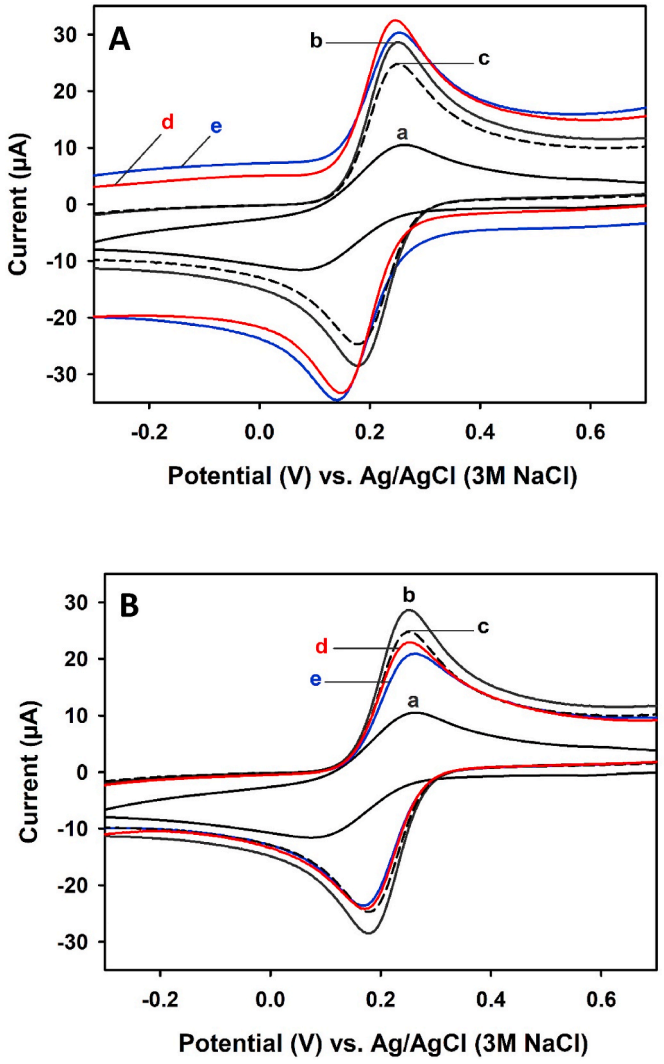

Fig. 3. (A) Cyclic voltammograms of (a) GCE, (b) GO/GCE, (c) *a*GO/GCE, (d) wAB/*a*GO/GCE and (e) BSA/wAB/*a*GO/GCE and (B) cyclic voltammograms of (a) GCE, (b) GO/GCE, (c) *a*GO/GCE, (d) oAB/*a*GO/GCE and (e) BSA/oAB/*a*GO/GCE with a scan rate of 50 mV/s in the presence of 1 mM of $K_3[Fe(CN)_6]$, 1 mM of $K_4[Fe(CN)_6]$ and 0.1 M of KCl.

SEM images for the *a*GO/GCE, wAB/*a*GO/GCE and oAB/*a*GO/GCE are demonstrated in Fig. S1. Activated graphene oxide (*a*GO) appears to have clear, sharp-edged and acicular shapes (Fig. S1A and S1A'). After wAB or oAB incubation, it was observed that it was covered with cloudy structures (Fig. S1B and S1C) [28].

After GO deposition onto the GCE's surface, carbon and oxygen contents were found in the mass ratio of 59.7% and 40.3%, respectively (Fig. S2A). With the functionalisation of GO/GCE with EDC and NHS, the rate of oxygen significantly decreased and the rate of carbon remarkably increased since the carbon ratio on the *a*GO/GCE is higher than oxygen (Fig. S2B). It was observed that the sulfur peaks emerged for both wAB/*a*GO/GCE and oAB/*a*GO/GCE with the immobilisation of wAB and oAB, respectively (Fig. S2C and S2D).

Although the proteins contain high amounts of nitrogen, they were not observed with EDX. Therefore, XPS, a more advanced surface characterisation technique, was used as appear in Fig. 4. C1s bonds between 284.48 – 285.68 eV and 285.98–286.78 eV are related to the graphitic and etheric structures, respectively. The weak C1s peaks at 288.58 and 290.48 eV and the strong O1s peak at 532.78 eV for GO/GCE belong to the carbonyl and carboxyl groups [29] and C–O (from carbonyl), respectively [30]. With the activation of GO/GCE, the C1s peak at 289.18 eV and the O1s peak at 531.78 eV indicate the presence of ester and amide groups on the surface, respectively [30,31]. In addition, the N1s core-level spectrum demonstrates a main peak component at 400.08 eV referred to the neutral amine groups, and a minor peak component at 402.48 eV attributed to the positively charged nitrogen species, respectively [32]. These findings showed that the electrode surface was successfully activated by EDC and NHS. After the wAB or oAB was modified on the surface of *a*GO/GCE, large increases in the overall N1s peaks observed for each electrode are related to amino acids in the structure of antibodies. Next, the emergence of S2p peaks is associated with C–S bonds in the structure of amino acids [33–35]. Furthermore, it is crucial to indicate that the N1s amine peak intensities in the wAB/*a*GO/GCE are much higher than in the oAB/*a*GO/GCE. Regardless of the conformation mutation, this could be associated with the increasing peak heights due to the interaction between the amine protons and the negatively charged redox couple for the wAB/*a*GO/GCE in CV characterisation.

Accordingly, well-matched CV, SEM, EDX and XPS results revealed that the developed biosensing platforms for detecting the wAG and oAG were produced accurately and appropriately.

3.2. Cyclic voltammetric characteristics of the developed systems

To elucidate the electrode reaction mechanisms between the nucleocapsid antigen proteins and the developed biosensing platforms, CV was used for both supporting electrolyte and antigen at 75 mV/s, and for antigen at increasing scan rates as appear in Fig. S3. The peak of the biosensing platforms at −60 mV irreversibly increased in the presence of wAG and oAG as shown in Fig. S3A. The logarithm of peak height ($\log(I_p$, μA)) and the logarithm of scan rate ($\log(\vartheta$, mV/s)) plotted to specify whether the wAG and oAG's relocation to the sensor surfaces was diffusion- or adsorption-controlled were $\log(I_p) = 1.190\log(\vartheta) - 1.487$ (R^2: 0.999) and $\log(I_p) = 1.109\log(\vartheta) + 0.723$ (R^2: 0.992) for wAG and

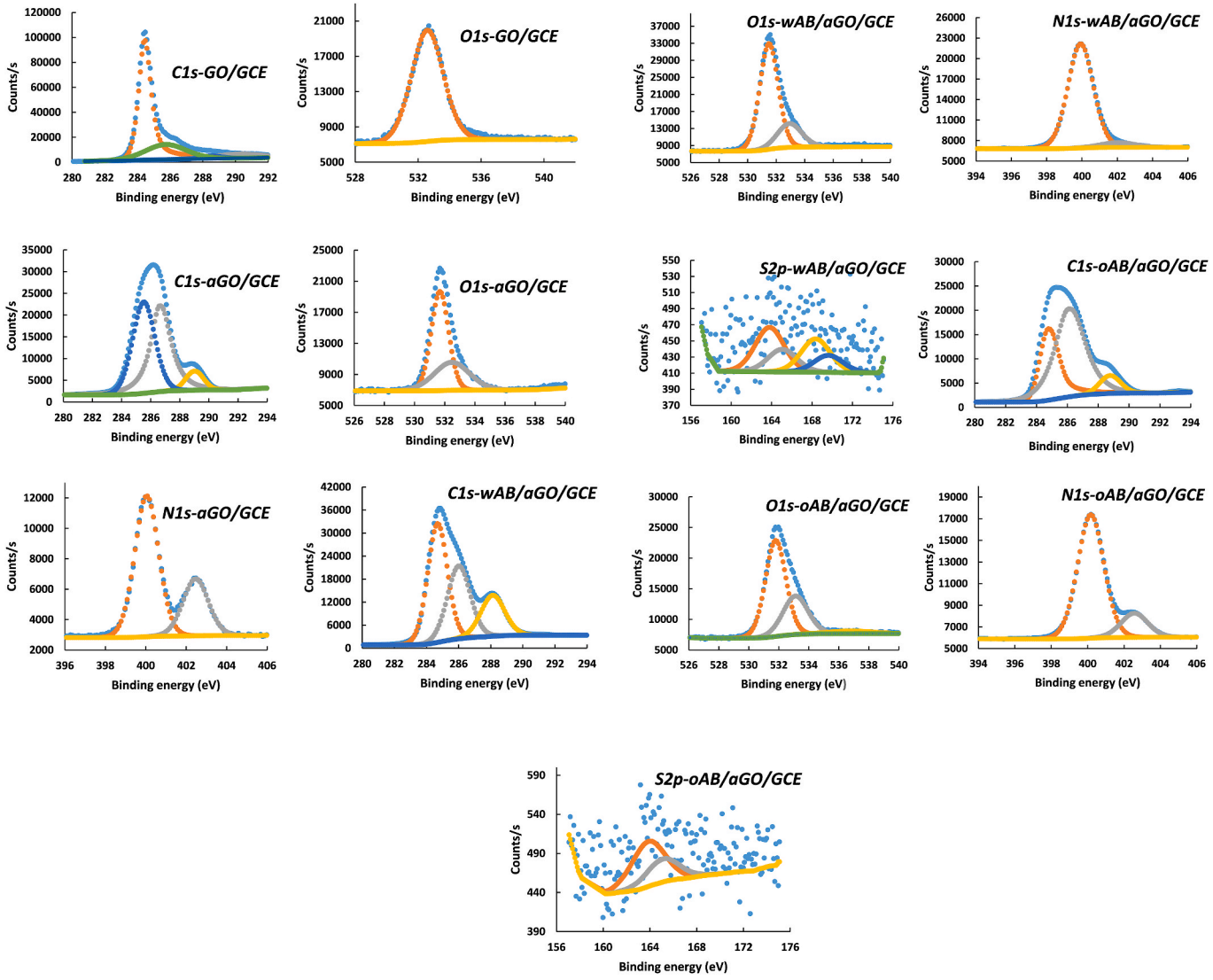

Fig. 4. XPS spectra for the GO/GCE, *a*GO/GCE, wAB/*a*GO/GCE and oAB/*a*GO/GCE. XPS analysis: Al Kα gun, 300 μm spot size, 50 eV pass energy, 0.1 eV energy step size.

oAG, respectively (Figs. S3B and S3C). The slopes of these equations revealed an adsorption-controlled electrode reaction in both systems.

3.3. Optimisation studies

Significant parameters having an effect upon the performance of BSA/wAB/*a*GO/GCE and BSA/oAB/*a*GO/GCE were optimised in the presence of 1 fg/mL of the related nucleocapsid antigen protein (Figs. S4 and S5). Among the results, the concentrations of GO and wAB, the EDC-NHS ratio (100 mM each), and the incubation times of wAB, EDC-NHS, BSA and wAG were determined to be 2.5 mg/mL, 20 μg/mL, 6 μL/14 μL, 30 min, 1.5 h, 10 min and 45 min for BSA/wAB/*a*GO/GCE, respectively (Fig. S4). All parameters are the same for BSA/wAB/*a*GO/GCE, only the ratio and incubation time of EDC-NHS are 16 μL/4 μL and 30 min, also respectively (Fig. S5). Supporting electrolyte of PBS solution (0.01 M pH 7.5) was used for all the measurements.

3.4. Validation of the method and sample application

Capacitive current based on the interaction between nucleocapsid antibody and antigen proteins increased in proportion to antigen proteins [35]. The SWV results and calibration curves for determining the wAG and oAG appear in Fig. 5. ΔI_P values were obtained by subtracting the corresponding biosensor's own signal from the incubated antigen signal. The developed biosensors, BSA/wAB/*a*GO/GCE and BSA/oAB/*a*GO/GCE, have limit of detection values and linear range intervals of 0.76 and 0.24 ag/mL (i.e. from the standard error of estimate) and 1 ag/mL–100 fg/mL and 1 ag/mL–10 fg/mL for determining wAG and oAG in 0.01 M (pH 7.5) of PBS solution, respectively.

The relative standard deviation values were found as 5.0% for BSA/wAB/*a*GO/GCE and 1.2% for BSA/oAB/*a*GO/GCE in the presence of 100 ag/mL of the wAG and oAG, respectively.

The proposed method was applied to nasopharyngeal swab samples for detecting wAG and oAG separately using BSA/wAB/*a*GO/GCE and BSA/oAB/*a*GO/GCE. Hereby, it was decided to set 1.3 and 9.1 μA current increase as threshold for wAG and oAG positive nasopharyngeal swab samples, respectively. The results showed that 27/30 wAG positive, 26/30 wAG negative, 24/25 oAG positive and 23/25 oAG negative samples were in agreement with RT-PCR analyses, depicting 90% and 96% sensitivity and 87% and 92% specificity for wAG and oAG, respectively. More importantly, it was investigated whether the produced biosensing platforms by using the cross-reactivity between wAB–oAG and oAB–wAG and the difference in current increases for wAG and oAG could be used interchangeably. For this purpose, 6

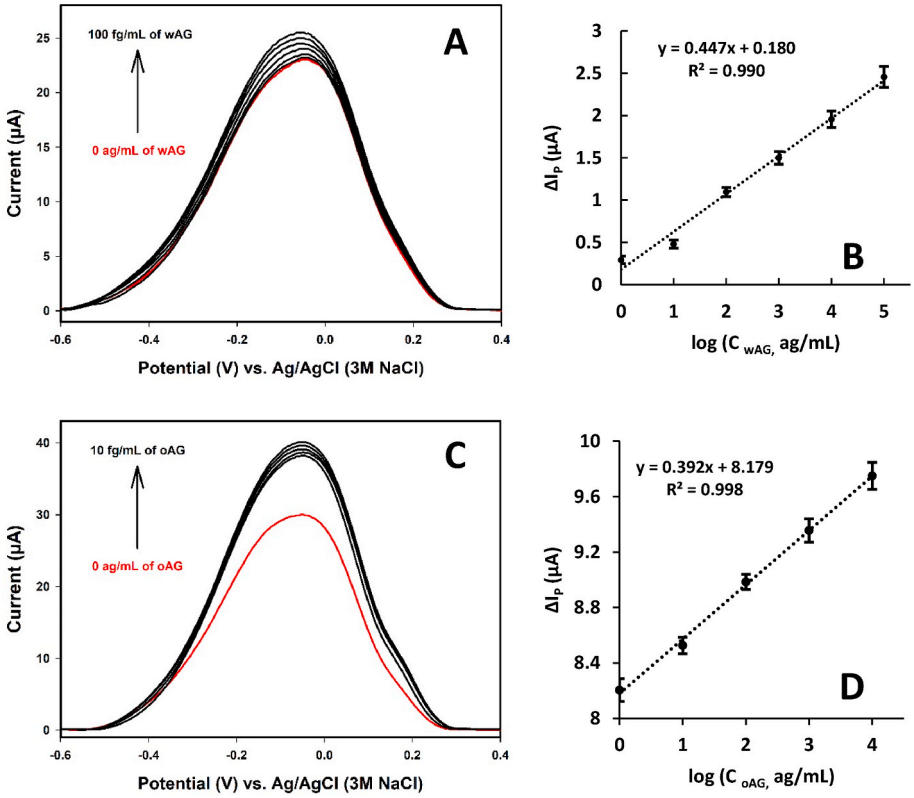

Fig. 5. (A, C) The square wave voltammograms and (B, D) the calibration curves (n = 3 for each concentration) for (A, B) BSA/wAB/*a*GO/GCE and (C, D) BSA/oAB/*a*GO/GCE in 0.01 M (pH 7.5) of PBS solution.

positive and 6 negative nasopharyngeal swab samples for each wAG and oAG were tested with both biosensors and it was observed that each platform was able to distinguish wildtype and omicron variant of SARS-CoV-2 nucleocapsid protein as appear in Fig. 6.

The obtained results showed that the BSA/oAB/*a*GO/GCE platform gave a more distinctive response than the BSA/wAB/*a*GO/GCE.

4. Conclusion

In this study, simple, easy-to-use, cost-effective, ultrasensitive and highly accurate two biosensing platforms are presented for detecting the wildtype and omicron variant of SARS-CoV-2 nucleocapsid protein in nasopharyngeal swab samples and the results show excellent sensitivity and specificity compared to RT-PCR. To our best knowledge, this is the first example to distinctively detect the nucleocapsid proteins of the wildtype and the omicron variant of the SARS-CoV-2 in real samples by any of the two sensors produced.

CV, SEM, EDX and XPS results of the biosensors have provided crucial information about the wildtype and omicron antigen and antibody structures. Although nucleocapsid proteins are less mutated, it has been observed that this could lead to misdiagnosis in electrochemical biosensing studies.

The electrochemical approach used here can be applied to different mutations of various viruses or biological materials, leading to the identification of different types of the same species.

Author contributions

Lokman Liv: Conceptualization, Methodology, Validation, Formal analysis, Investigation, Writing – original draft, Writing - review & editing, Visualization, Supervision. **Aysu Baş:** Visualization, Validation, Investigation.

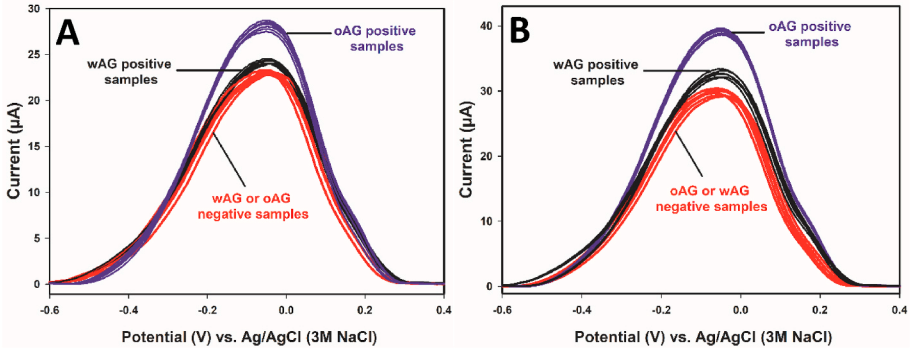

Fig. 6. The SWV voltammograms of nasopharyngeal swab samples containing wAG or oAG with a single biosensing platform: (A) BSA/wAB/*a*GO/GCE and (B) BSA/oAB/*a*GO/GCE. Negative samples comprised of 3 negative wAG and 3 negative oAG nasopharyngeal swab samples for both voltammograms.

Data availability

The authors do not have permission to share data.

Acknowledgements

The study was performed at Electrochemistry Laboratory, National Metrology Institute of Turkey (TUBITAK UME). The authors would like to thank Burcu Şebnem Sobacı (TUBITAK UME-Electrochemistry Laboratory) for some voltammetric experiments, Erman Karakuş (TUBITAK UME-Organic Chemistry Laboratory) for SEM and EDX measurements, Ayşegül Erdoğan and Meral Esen (Ege University Application and Research Center for Testing and Analysis-EGE-MATAL) for XPS measurements and Tanıl Kocagöz for supplying the clinical samples which were formerly studied by RT-PCR. The graphical abstract, Figs. 1 and 2 were created by BioRender software.

Appendix A. Supplementary data

Supplementary data to this article can be found online at https://doi.org/10.1016/j.ab.2022.114898.

References

[1] C. Sohrabi, Z. Alsafi, N. O'Neill, M. Khan, A. Kerwan, A. Al-Jabir, C. Iosifidis, R. Agha, A review of the 2019 novel coronavirus (COVID-19), Int. J. Surg. 76 (2020) 71–76.
[2] F. Wu, S. Zhao, B. Yu, Y. Chen, W. Wang, Z. Song, Y. Hu, Z. Tao, J. Tian, Y. Pei, M. Yuan, Y. Zhang, F. Dai, Y. Liu, Q. Wang, J. Zheng, L. Xu, E.C. Holmes, Y. Zhang, A new coronavirus associated with human respiratory disease in China, Nature 579 (2020) 265–269.
[3] IMF, Update of the IMF Global Debt Database, 2021, 2021, https://www.imf.org/en/News/Seminars/Conferences/2021/12/15/2021-update-of-the-imf-global-debt-database. (Accessed 2 June 2022).
[4] WHO, WHO Coronavirus (COVID-19) Dashboard, 2022. https://covid19.who.int/. (Accessed 2 June 2022).
[5] A. Aleem, A.B. Akbar Samad, A.K. Slenker, Emerging Variants of SARS-CoV-2 and Novel Therapeutics against Coronavirus (COVID-19), 2022. https://www.ncbi.nlm.nih.gov/books/NBK570580/. (Accessed 2 June 2022).
[6] WHO, Tracking SARS-CoV-2 Variants, 2022. https://www.who.int/activities/tracking-SARS-CoV-2-variants. (Accessed 2 June 2022).
[7] J. Chen, R. Wang, N.B. Gilby, G.W. Wei, Omicron (B.1.1.529): infectivity, vaccine breakthrough, and antibody resistance, ArXiv 1 (2021), 2112.01318v1.
[8] N. Andrews, J. Stowe, F. Kirsebom, S. Toffa, T. Rickeard, E. Gallagher, C. Gower, M. Kall, N. Groves, A. O'Connell, D. Simons, P.B. Blomquist, A. Zaidi, S. Nash, N.I. B.A. Aziz, S. Thelwall, G. Dabrera, R. Myers, G. Amirthalingam, S. Gharbia, J. C. Barrett, R. Elson, S.N. Ladhani, N. Ferguson, M. Zambon, C.N.J. Campbell, K. Brown, S. Hopkins, M. Chand, M. Ramsay, J.L. Bernal, Covid-19 vaccine effectiveness against the omicron (B.1.1.529) variant, N. Engl. J. Med. 386 (2022) 1532–1546.
[9] FDA, SARS-CoV-2 Viral Mutations: Impact on COVID-19 Tests, 2022. https://www.fda.gov/medical-devices/coronavirus-covid-19-and-medical-devices/sars-cov-2-viral-mutations-impact-covid-19-tests#omicronvariantimpact. (Accessed 6 June 2022).
[10] Y. Li, L. Yao, J. Li, L. Chen, Y. Song, Z. Cai, C. Yang, Stability issues of RT-PCR testing of SARS-CoV-2 for hospitalized patients clinically diagnosed with COVID-19, J. Med. Virol. 92 (2020) 903–908.
[11] L. Lan, D. Xu, G. Ye, C. Xia, S. Wang, Y. Li, H. Xu, Positive RT-PCR test results in patients recovered from COVID-19, JAMA 323 (2020) 1502–1503.
[12] Z. Wang, Y. Chen, J. Yang, Y. Han, J. Shi, S. Zhan, R. Peng, R. Li, R. Zhang, J. Li, R. Zhang, External quality assessment for molecular detection of severe acute respiratory syndrome coronavirus 2 (SARS-CoV-2) in clinical laboratories, J. Mol. Diagn. 23 (2021) 19–28.
[13] B.G. Andryukov, Six decades of lateral flow immunoassay: from determining metabolic markers to diagnosing COVID-19, AIMS Microbiol 6 (2020) 280–304.
[14] H. Han, C. Wang, X. Yang, S. Zheng, X. Cheng, Z. Liu, B. Zhao, R. Xiao, Rapid field determination of SARS-CoV-2 by a colorimetric and fluorescent dual-functional lateral flow immunoassay biosensor, Sensor. Actuat. B-Chem. 351 (2022), 130897.
[15] T. Wen, C. Huang, F.J. Shi, X.Y. Zeng, T. Lu, S.N. Ding, Y.J. Jiao, Development of a lateral flow immunoassay strip for rapid detection of IgG antibody against SARS-CoV-2 virus, Analyst 145 (2020) 5345.
[16] W.H. Khan, N. Khan, A. Mishra, S. Gupta, V. Bansode, D. Mehta, R. Bhambure, M. A. Ansari, S. Das, A.S. Rathore, Dimerization of SARS-CoV-2 nucleocapsid protein affects sensitivity of ELISA based diagnostics of COVID-19, Int. J. Biol. Macromol. 200 (2022) 428–437.
[17] L. Liv, Electrochemical immunosensor platform based on gold-clusters, cysteamine and glutaraldehyde modified electrode for diagnosing COVID-19, Microchem. J. 168 (2021), 106445.
[18] L. Liv, G. Çoban, N. Nakiboglu, T. Kocagöz, A rapid, ultrasensitive voltammetric biosensor for determining SARS-CoV-2 spike protein in real samples, Biosens. Bioelectron. 192 (2021), 113497.
[19] L. Liv, M. Yener, G. Çoban, Ş.A. Can, Electrochemical biosensing platform based on hydrogen bonding for detection of the SARS-CoV-2 spike antibody, Anal. Bioanal. Chem. 414 (2022) 1313–1322.
[20] L. Liv, H. Kayabay, An electrochemical biosensing platform for the SARS-CoV-2 spike antibody detection based on the functionalised sars-cov-2 spike antigen modified electrode, ChemistrySelect 7 (2022), e202200256.
[21] A. Raziq, A. Kidakova, R. Boroznjak, J. Reut, A. Opik, V. Syritski, Development of a portable MIP-based electrochemical sensor for detection of SARS-CoV-2 antigen, Biosens. Bioelectron. 178 (2021), 113029.
[22] S. Eissa, M. Zourob, Development of a low-cost cotton-tipped electrochemical immunosensor for the detection of SARS-CoV-2, Anal. Chem. 93 (2021) 1826–1833.
[23] M. Alafeef, K. Dighe, P. Moitra, D. Pan, Rapid, ultrasensitive, and quantitative detection of SARS-CoV-2 using antisense oligonucleotides directed electrochemical biosensor chip, ACS Nano 14 (2020) 17028–17045.
[24] B.S. Vadlamani, T. Uppal, S.C. Verma, M. Misra, Functionalized TiO_2 nanotube-based electrochemical biosensor for rapid detection of SARS-CoV-2, Sensors 20 (2020) 5871.
[25] Q. Pagneux, A. Roussel, H. Saada, C. Cambillau, B. Amigues, V. Delauzun, I. Engelmann, E.K. Alidjinou, J. Ogiez, A.S. Rolland, E. Faure, J. Poissy, A. Duhamel, R. Boukherroub, D. Devos, S. Szunerits, SARS-CoV-2 detection using a nanobody-functionalized voltammetric device, Commun. Med. 2 (2022) 56.
[26] C. Huang, T. Wen, F.J. Shi, X.Y. Zeng, Y.J. Jiao, Rapid detection of IgM antibodies against the SARS-CoV-2 virus via colloidal gold nanoparticle-based lateral-flow assay, ACS Omega 5 (2020) 12550–12556.
[27] B.A. Johnson, Y. Zhou, K.G. Lokugamage, M.N. Vu, N. Bopp, P.A. Crocquet-Valdes, B. Kalveram, C. Schindewolf, Y. Liu, D. Scharton, J.A. Plante, X. Xie, P. Aguilar, S. C. Weaver, P.Y. Shi, D.H. Walker, A.L. Routh, K.S. Plante, V.D. Menachery, Nucleocapsid mutations in SARS-CoV-2 augment replication and pathogenesis, bioRxiv (2022) 2021, 10.14.464390.
[28] O. Parkash, C.Y. Yean, R.H. Shueb, Screen printed carbon electrode based electrochemical immunosensor for the detection of dengue NS1 antigen, Diagnostics 4 (2014) 165–180.
[29] G. Ilangovan, K.C. Pillai, Electrochemical and XPS characterization of glassy carbon electrode surface effects on the preparation of a monomeric molybdate(VI)-modified electrode, Langmuir 13 (1997) 566–575.
[30] R. Sadri, M. Hosseini, S.N. Kazi, S. Bagheri, N. Zubir, K.H. Solangi, T. Zaharinie, A. Badarudin, A bio-based, facile approach for the preparation of covalently functionalized carbon nanotubes aqueous suspensions and their potential as heat transfer fluids, J. Colloid Interface Sci. 504 (2017) 115–123.
[31] J. Peeling, F.E. Hruska, D.M. McKinnon, M.S. Chauhan, N.S. McIntyre, ESCA studies of the uracil base. The effect of methylation, thionation, and ionization on charge distribution, Can. J. Chem. 56 (1978) 2405–2411.
[32] S. Yuan, J. Gu, Y. Zheng, W. Jiang, B. Liang, S.O. Pehkonen, Purification of phenol-contaminated water by adsorption with quaternized poly(dimethylaminopropyl methacrylamide)-grafted PVBC microspheres, J. Mater. Chem. 3 (2015) 4620–4636.
[33] N. Li, A.M. Chow, H.V.S. Ganesh, M. Ratnam, I.R. Brown, K. Kerman, Diazonium-modified screen-printed electrodes for immunosensing growth hormone in blood samples, Biosensors 9 (2019) 88.
[34] F. Xu, S. Ren, J. Li, X. Bi, Y. Gu, Molecular assembly of a durable HRP-AuNPs/PEDOT:BSA/Pt biosensor with detailed characterizations, Sensors 18 (2018) 1823.
[35] N. Olgaç, Y. Şahin, L. Liv, Development and characterisation of cysteine-based gold electrodes for the electrochemical biosensing of the SARS-CoV-2 spike antigen, Analyst, doi:10.1039/D2AN01225A, In press.